PNAS
www.pnas.org

Supplementary Information for

Mechanism of β-arrestin recruitment by the μ-opioid G-Protein Coupled Receptor

Amirhossein Mafi, Soo-Kyung Kim, and William A. Goddard III*

* corresponding author
Email: wag@caltech.edu

This PDF file includes:

SI Methods
Figures S1 to S9
Tables S1
Legends for Movies S1 to S4
SI References

Other supplementary materials for this manuscript include the following:

Movies S1 to S4

www.pnas.org/cgi/doi/10.1073/pnas.1918264117

SI Methods

pp-Rhod-arrestin 1 complex preparation.

Seven residues were not fully resolved in the *chain A* of the recent crystal structure (PDB ID:5W0P)(*1*) including the full sequence of 324-330 in the C-tail of pp-rhod and side chains of residue 2075 and 2080 in the arrestin-1. We added the missing side chains using Swiss-pdbviewer(*2*), where during the process we also reconstructed the side chains. We built the missing sequence from 325-329 using MODELLER program(*3*) using the chain A of crystal rhod-arrestin complex (pdb ID:4ZWJ)(*4*). We also removed the T4L protein and N-acetylglucosamine that had been added to promote crystallization. To refine the 7 added residues on the C-tail, we subjected the complex to 1000 steps of energy minimization using steepest descents and subsequently applied 80 cycles of temperature annealing over 4 ns, where all residues including the added ones on the C-tail were heated from 0 to 25 to 600K for 25, 100, 310, 450, and 600 over 20 ps and then cooled back to 310 over 30 ps. During this process, all backbone atoms except for residues 324-330 in the C-tail were restrained with the force constant of 9.6 kcal.mol^{-1}.Å^{-2} in order that the atoms resolved in the crystal structure not be disturbed, since we wanted only to refine the atoms not resolved. We embedded this refined complex in a palmitoyl-oleoyl-phosphatidylcholine (POPC) bilayer composed of 356 POPC molecules and then solvated the system with ~40K water molecules. We neutralized the system and added 0.15mM NaCl to maintain the biological salt concentration, which resulted to a simulation box of 123x104x138 Å^3. Subsequently, we minimized the system for 5000 steps of energy minimization using the steepest descent algorithm and then equilibrated the complex for 520 ps of NVT followed by 700 ps NPT simulations where positional restraints were placed on the heavy atoms with a force constant of 9.6 kcal.mol^{-1}.Å^{-2}. Then, we performed 450 ns of NPT simulation in which we removed the positional restraints on the heavy atoms and placed restraints on the backbone atoms to refine the interactions without changing the shape of the crystal structure. This refined complex differed from the crystal structure by RMSD=0.3 Å. It was used as a template for comparison and modelling of the pp-μOR-βarr2 interface.

Modeling of human pp-μOR in complex with morphine

First, we used the activated mouse-μOR structure [PDB ID: 5C1M](*5*) as a template for GEnSeMBLE predictions(*6*) to model the activated structure for the human-μOR. Briefly, the GEnSeMBLE procedure(*6*) starts with the tilts for the 7 helical TM domains of mouse-μOR as a template and examines all possible tilts and rotations of these helices up to 10° for the polar angle and up to 30° for the other angles. This leads to 13 trillion combinations for each of which we estimate the energy considering only pair-wise interactions between the seven TM, with the side chains optimized for interhelical interactions using SCREAM(*7*).Then for the 1000 predicted best combinations, we built 7-TM bundles while re-optimizing the side chains for interhelical interactions independently for each of the 1000 and carrying out conjugate gradient minimization to remove bad contacts. From this 1000 cases we selected the 25 lowest-energy packings as the ensemble for docking ligands.

Next we predicted the binding site of morphine to each of these 25 packings using the DarwinDock procedure(*8*). Briefly, the optimum morphine conformations from the X-ray structure was minimized and then docked to each of the 25 packings of 7TM bundles in

the human-μOR. For each ligand-μOR combination, we replaced the 6 hydrophobic residues with Ala and then examined 50,000 poses without energy evaluations. Instead we group them into ~ 2000 Voronoi families using RMSD. Then we evaluated energies for the family heads. Then for the best 10%, we evaluated the energies of all children, from which we selected the best 100 by energy. Then we used SCREAM to convert back from Ala for the 6 hydrophobic residues so that each pose has the optimum set of side chains, which are different for each pose. Then we selected the best few binding poses by assessing the binding energy. Next we compared the 25×100=2500 binding energies using a unified binding site to select the best 10 structures, which we then compared to select the best combination of ligand-μOR coupling.

Using MODELLER(*3*), we added the native sequence of the long C-tail and connected to the last residue of the H8 helix on human MOR. Subsequently, we phosphorylated all Serine and Threonine residues in the C-tail to obtain the full degree of phosphorylation.

This human-μOR-morphine complex was used to match the DAMGO and TRV130.

Refinement of the pp-C tail of the μOR

To model the inactive βarr2- pp- μOR-morphine complex, we started with the crystal structure of inactive bovine arrestin-3 (pdb ID: 3P2D)(*9*) to use as an input for the SWISS-MODEL server(*10*) to predict the *inactive* structure of the human βarr2 in accord with homology modeling. Subsequently, we superimposed the resulting structure of βarr2 and pp-μOR-morphine separately onto the arrestin-1 and pp-rhod of our optimized pp-rhod-arrestine1 complex, respectively. To refine the pp-C-tail conformation and the interaction with βarr2, we subjected the complex to 1000 steps of energy minimization using the steepest descents algorithm and subsequently carried out 400 cycles of temperature annealing over 20 ns. Here all residues including the added ones on the C-tail were heated from 0 to 25 to 600K with the sequence of 25, 100, 310, 450, and 600 over 20 ps and then cooled back to 310 over 30 ps. During this process, all backbone atoms except for residues 341-400 on the pp-C-tail, were restrained with a force constant of 9.6 kcal.mol-^{1}.Å^{-2} to refine the interactions and side chains. In addition, we placed restraints with a force constant of 1.2 kcal.mol^{-1}.Å^{-2} on the distances between pS357-R157$^{\beta arr2}$, pS358-K13$^{\beta arr2}$, pS365-R47$^{\beta arr2}$, pT366-R47$^{\beta arr2}$, pT372-K45$^{\beta arr2}$, pS395-K6$^{\beta arr2}$, and pT385-R102$^{\beta arr2}$ to expedite forming salt bridges between the pairs. We immersed this complex in a POPC bilayer composed of 356 of POPC molecules and then solvated with ~40K water molecules. We neutralized the system and added 0.15mM NaCl to maintain the biological salt concentration. This resulted in a simulation box of 123x104x138 Å^{3}, with ~180K atoms. Subsequently, we minimized the system with 5000 steps of energy minimization using the steepest descents algorithm and subsequently equilibrated the complex by performing 20 ps of NVT followed by 10.2 ns of NPT simulations, where positional restraints were placed on the heavy atoms with a force constant of 9.6 kcal.mol^{-1}.Å^{-2} which was gradually reduced to 0 kcal.mol^{-1}.Å^{-2}. Then, we performed 36.6 ns of NPT simulation where we removed the positional restraints on the heavy atoms but we used a set of harmonic restraints on the inter-helical hydrogen bonds in order to relax the protein structure while ensuring that the helical domains are stable and intact over the course of simulation. The distance between N (i+4) and C (i) atoms of the residues in the helices was restrained at a distance of 4.1 Å using a force constant of ~1.2 kcal.mol^{-1}Å^{-2}. To refine the

conformation of the pp-C tail, we performed several short metaMD simulations (described below) for an overall time of ~380ns to examine formation of several potential salt bridges between the phosphorylated serine and threonine residues on the C tail and the positively charged residues on the N-domain of βarr2. The purpose of these calculations was to prepare the conformation of C-tail to properly interact with the N-domain of *activated* βarr2. Thus, we did not fully converge these free energies. Rather, we just encouraged several potential salt bridges to be made by following several cycles (at least one cycle) of forming and breaking those salt bridges in a limited number of pathways. This procedure is sufficient to perturb the energy of system in reduced time scale to refine the pp-C tail conformation while searching for additional salt bridges that might couple tightly to the N-domain of inactive βarr2 with the pp-C tail. This technique, using short metaMD simulations without the need of free energy convergence, was used before to assess the energetics of different pathways of ligand-protein binding (*11*, *12*).

Once these preliminary calculations were done, we removed the inactive form of βarr2 and replaced it with the activated form of βarr2 in order to optimize the fully engaged βarr2-pp-μOR-agonists (our desired complexes) as described below.

Details of metaMD simulations

To refine the conformation of pp-C tail to engage tightly the βarr2, we performed several short metaMD simulations to encourage forming several salt bridge interactions between the pS and pT residues form the pp-C tail to the positively charged residues on the N-domain.

Starting from the pre-equilibrated structure obtained from the ~67ns of MD simulations, we applied the well-tempered metaMD(*13*) bias force on the distance between pT396(P)-R95$^{\beta arr2}$(CZ), in which they were 25.6Å apart from each other.
We performed a well-tempered metaMD simulation for ~88ns to promote the formation of the salt bridge between the pair (shown in Figure S9A), which substantially reduced the system energy by ~-17kcal/mol (shown in Figure S9B).
The bias was used a Gaussian width of 1 Å, an initial Gaussian amplitude of 0.6 kcal/mol, a deposition period of 1.0 ps, and a bias factor of 20. To expedite the sampling process, we imposed a harmonic upper wall with a force constant of ~24 kcal.mol^{-1}Å^{-2} at a distance of 25.0 Å to limit the sampling space accessible during the simulation. During this calculation, we also introduced a harmonic restraint on the important salt bridges that were already formed from the previous calculations. Here, we placed a harmonic restraint on the distance between D179^{ICL2} (CG)-K134$^{\beta arr2}$ (NZ), at a distance of 3.5 Å and force constants of ~1.2 kcal.mol^{-1}Å^{-2} to ensure that this interaction is intact over the perturbations that metaMD calculation causes.
We repeated the same strategy for several potential salt bridges (summarized in the Table S1). The well-tempered metaMD simulations were implemented using the PLUMED 2.4.1(*14*). The free energy profile resulted from these calculations are represented in Figure S9.

Modeling of pp- μOR-morphine to complex with the *active* βarr2.

To model the active βarr2-pp-μOR-morphine complex, we used the crystal structure of active bovine arrestin-3 as a template for homology modeling with MODELELR(*3*).

Subsequently, we superimposed the βarr2 and refined pp-μOR-morphine (from the previous step) structures onto the arrestin-1 and pp-rhod of the optimized pp-rhod-arrestine1 complex, respectively. We immersed this complex in a POPC bilayer composed of 356 POPC molecules and then solvated it with ~40K water molecules. We neutralized the system and added 0.15mM NaCl to maintain the biological salt concentration, which resulted in a simulation box of 123x104x138 $Å^3$ with ~180K atoms. Subsequently, we minimized the system for 5000 steps of steepest descents and subsequently equilibrated the complex by performing 1.1 ns of NVT followed by 9 ns of NPT simulations, where positional restraints were placed on the heavy atoms with a force constant of 9.6 $kcal.mol^{-1}.Å^{-2}$ which was gradually reduced to 0 $kcal.mol^{-1}.Å^{-2}$. Finally, we removed all restraints and performed a 500 ns of NPT simulation, which was used to make Figure 2 in this paper. To test our model, we independently performed a new set of simulations for ~510ns where we reassigned the velocities.

To test the role of the lipid anchoring from the C-edge of the βarr2, we performed another simulation in which the C-edge of the βarr2 lacked any contacts with the membrane bilayer. To perform this simulation, we pushed the C-edge into the water and subsequently carried out a ~200ns MD simulation.

Modeling of pp-μOR-DAMGO in complex with the *active* βarr2.

To match DAMGO to the activated pp-μOR resulting from the previous calculation, we first superimposed the human pμOR to the recent activated mouse-μOR obtained by cryo-EM (pdb id: 6DDF)(*15*), Needleman-Wunsch sequence alignment algorithm(*16*) with the BLOSUM-62 matrix. Then, to locate and optimize the binding interactions between human-μOR and DAMGO, we subjected the complex to 1000 steps of energy minimization with steepest descents and subsequently to 500 cycles of temperature annealing over 5 ns, where all residues and DAMGO were heated from 0 to 25 to 600K with the sequence of 25, 100, 310, 450, and 600 over 20 ps and then cooled back to 310 over 30 ps. During this calculation, all backbone atoms of proteins and DAMGO heavy atoms were restrained with force constants of 9.6 and 2.4 $kcal.mol^{-1}.Å^{-2}$, respectively. Then, we superimposed the resulted complex pp-μOR-DAMGO onto our βarr2-pp-μOR-morphine to build the βarr2-pp-μOR-DAMGO complex. We immersed this complex in a POPC bilayer composed of 356 of POPC molecules and then solvated with ~40K water molecules. We neutralized the system and then we added 0.15mM NaCl to maintain the biological salt concentration, which resulted in a simulation box of 123x104x138 $Å^3$. (180K atoms). Subsequently, we minimized the system with 1000 steps of using steepest descents and subsequently equilibrated the complex with 1.1 ns of NVT followed by 2.2 ns of NPT simulation where positional restraints were placed on the heavy atoms with a force constant of 9.6 $kcal.mol^{-1}.Å^{-2}$ which was gradually reduced to 0 $kcal.mol^{-1}.Å^{-2}$. Finally, we removed all restraints and performed a 500 ns of NPT simulation, which was used to make Figure 1 in this paper.

Umbrella sampling MD for finding the activation pathway of βarr2.

To find the activation pathway of βarr2, we assessed the energetics of decoupling the βarr2 from the activated complex by pulling it towards the solution inside the cell using the umbrella sampling method. (*17*, *18*) We inserted the bias forces on the distance along the z-component between the center of mass of Cαs in the pp-μOR for the residues 54-340 and

the center of mass of Cαs in βarr2. To do this, we sampled center of mass distances from 43-64 Å using 1Å increment in the z-component, which results to 23 separate windows/configurations. To find these different configurations, we gradually pulled the βarr2 away from the pp-μOR over the course of ~10 ns by applying the force constant of 0.48 kcal.mol^{-1}.Å^{-2} and a pull rate of 0.005Å.ps^{-1}. In these windows, while the pp-μOR was embedded in 356 POPC molecules, the βarr2 was solvated in a larger thickness of water including ~53K water molecules to facilitate study of βarr2 penetration. Then, we added enough counter ions to neutralize the system and added 0.15M of NaCl on top of that. Each window was subsequently subjected to a 1ns of NPT simulation, where we applied the restraint (3.6 kcal.mol^{-1}Å^{-2}) on the distance between the center of mass of Cαs in the pp-μOR for the residues 54-340 and the center of mass of Cαs in βarr2 to relax the system and prepare it for the final free energy calculation. Finally, we performed a 10ns of NPT simulation with time step size of 2.0 fs on each window, 230ns for all windows in total, with applying the same restraints on the distance between the center of mass of Cαs in the pp-μOR for the residues 54-340 and the center of mass of Cαs in βarr2 to evaluate the free energy. The free energy profile (Figure 1) was obtained by the weighted histogram analysis method (WHAM)(*19*). The statistical errors were evaluated by the bootstrap method(*20*) as shaded with pink in the Figure 4A. Movies S1-S4 were made from this calculation using UCSF Chimera(*21*). We repeated the same calculations for the recruitment of βarr2 by pp-μOR bound to DAMGO and TRV130 to assess the binding affinity.

Modeling of pp-μOR-TRV130 in complex with the *active* βarr2.

To build the complex of βarr2- pp-μOR-TRV130, we first matched TRV130 to the active conformation of human-μOR obtained from the GENSEMBLE calculation. Then, we superimposed the μOR-TRV130 complex to our optimized Gi-mouse-μOR-DAMGO(*22*) complex to build an activated state of Gi-μOR-TRV130. We immersed this complex in a POPC bilayer composed of 277 of POPC molecules and then solvated with ~32K water molecules. We neutralized the system and then added 0.15mM NaCl to maintain the biological salt concentration, which resulted to a simulation box of 101x101x146 Å^3. Subsequently, we minimized the system with 2000 steps of steepest descents and subsequently equilibrated the complex by performing a 1.2ns of NVT followed by a 7ns of NPT simulation, where positional restraints were placed on the heavy atoms with a force constant of 9.6 kcal.mol^{-1}.Å^{-2} which was gradually reduced to 0 kcal.mol^{-1}.Å^{-2}. We then performed another 80ns of NPT simulation, where we removed all restraints from the heavy atoms belonging to the protein while we kept strong restraints (2.4 kcal.mol^{-1}.Å^{-2}) on the heavy atoms of the TRV130. The purpose of this calculation was to allow the protein side chains to optimize and find the right interactions with the TRV130. Following that, we removed all restraints and performed a 240 ns of NPT simulation to relax the Gi- μOR-TRV130 complex. Figure 5 was made using the results of this calculation.

We then removed the Gi protein from our optimized Gi-μOR-TRV130 complex and immersed in this complex in a POPC bilayer composed of 164 of POPC molecules and then solvated with ~14K water molecules. We neutralized the system and then we added 0.15mM NaCl to maintain the biological salt concentration, which resulted in a simulation box of 80x80x107 Å^3. Subsequently, we minimized the system for 1000 steps of steepest descents and subsequently equilibrated the complex by performing a 1.0ns of NVT

followed by a 7ns of NPT simulation where positional restraints were placed on the heavy atoms with a force constant of 9.6 kcal.mol^{-1}.Å^{-2} that was gradually reduced to 0 kcal.mol^{-1}.Å^{-2}. We then performed another 400ns of NPT simulation, where we removed all restraints from the heavy atoms belonging to the protein while we kept strong restraints (2.4 kcal.mol^{-1}.Å^{-2}) on the heavy atoms of TRV130. The purpose of this calculation was to allow the intracellular and extracellular portions of the μOR to readjust in order to recruit βarr2. Following that, we removed all restraints and performed a ~100ns of NPT simulation to relax the μOR-TRV130 complex.

We subsequently used the optimized μOR-TRV130 complex and superimposed it to our optimized βarr2-pp-μOR-DAMGO to add the pp-C tail and also to include the active state of βarr2 into our model. We immersed the βarr2-pp-μOR-TRV130 complex in a POPC bilayer composed of 356 of POPC molecules and then solvated with ~40K water molecules. We neutralized the system and then added 0.15mM NaCl to maintain the biological salt concentration, which resulted to a simulation box of 123x104x138 Å^3. Subsequently, we minimized the system for 1200 steps of steepest descents and subsequently equilibrated the complex by performing 60ps of NVT followed by 650ps of NPT simulation where positional restraints were placed on the heavy atoms with a force constant of 9.6 kcal.mol^{-1}.Å^{-2} and gradually reduced to 0 kcal.mol^{-1}.Å^{-2}. Finally, we removed all restraints and performed a 500 ns of NPT simulation. This was used to make Figure 6 in this paper.

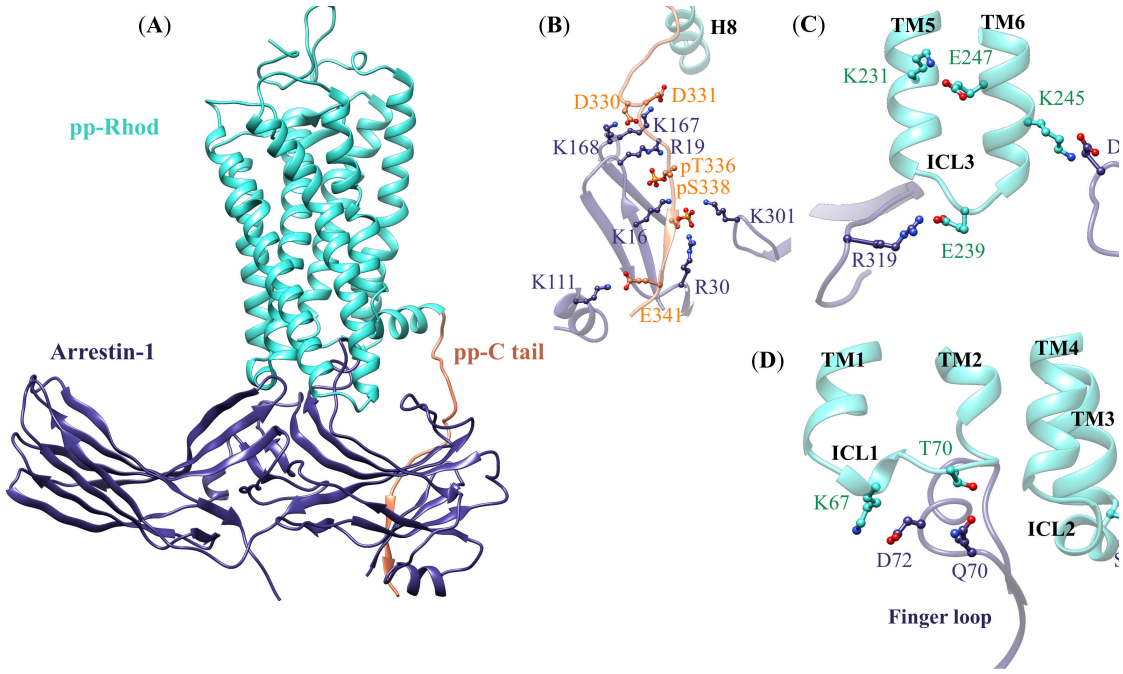

Fig. S1. Activated structure of arrestin-1 mediated by pp-rhod refined by MD simulation. (A) The overall view of the pp-rhod-arrestin-1 after 450ns of MD simulation, leading to 0.3Å RMSD (in respect to the Cα atoms) with the crystal structure (PDB ID: 5W0P), which are in excellent agreement. (B) Ionic interactions from arrestin-1 to the pp-C tail, where mostly involve between negatively charged residues on the C-tail residues and the positively charged residues on the N-domain of arrestin-1. (C) Anchoring from R319 on the back loop to E239 on the ICL3 and also a salt bridge from K245 to D163. These strong interactions coordinate TM5 to couple with TM6 by forming a charge-charge interaction from K231 to E247. (D) Anchoring from D254 and S252 on the C-loop to K141 on the ICL2. Besides, we find that the finger loop interacts strongly with ICL1 by forming a salt bridge from D72 to K67 and also from Q70 to T70. Interestingly, the anchors on ICL2 and ICL3 formed in an opposite electrostatic arrangement, negative-positive attraction for the ICL3 and positive-negative attraction for the ICL2, compared to the activated βarr2-pp-μOR complex. This may explain why pp-μOR does not intend to recruit the visual arrestins.

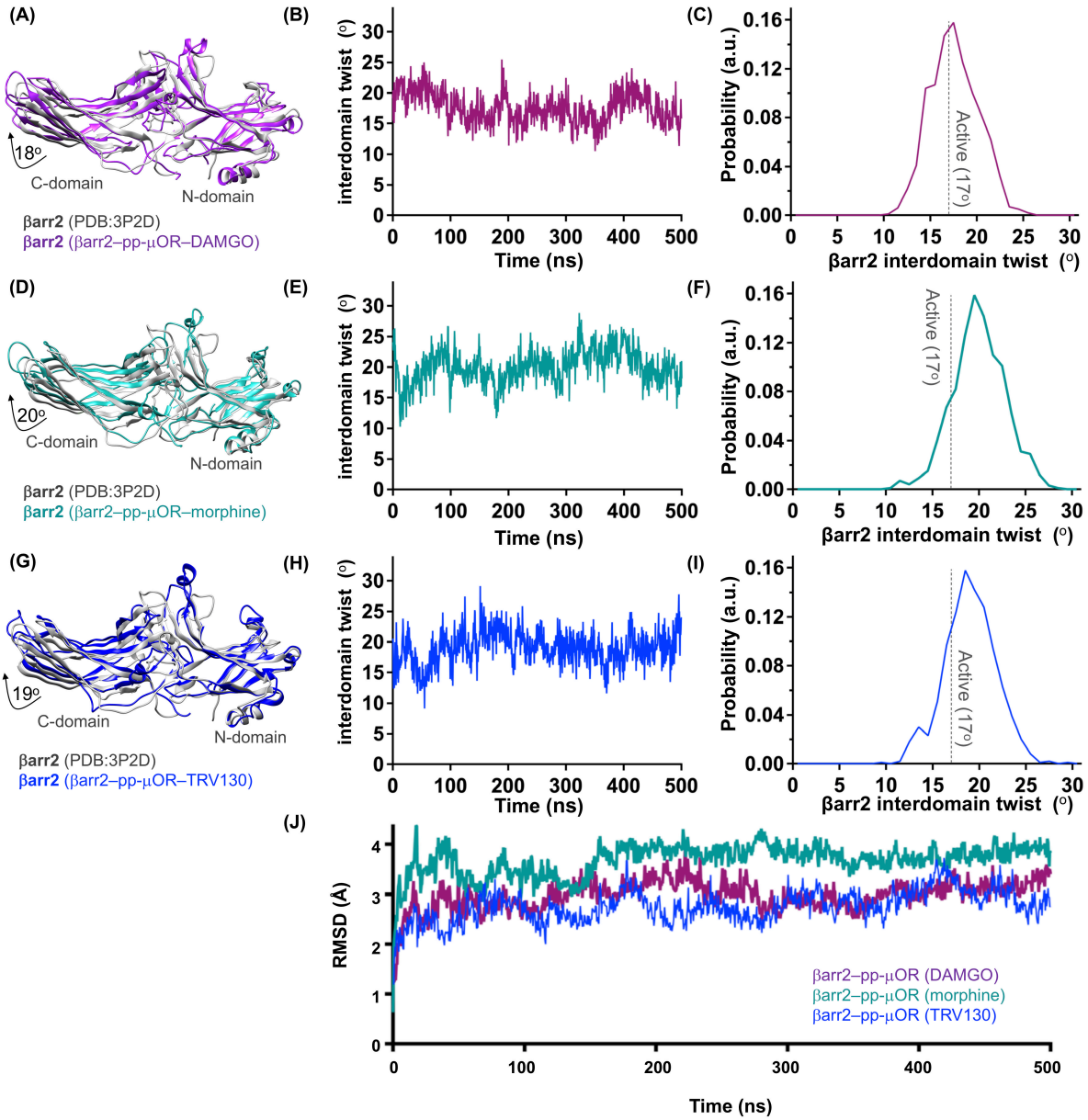

Fig. S2. Analysis of the conformation of the βarr2 upon engaging the 7TM core of the pp-μOR in the presence of DAMGO (full), morphine (partial), and TRV130 (biased) agonist for the coupling of the βarr2. Superimposed N-domain of the active (obtained from our MD simulation) to the inactive (resolved in experiment, PDB 3PD2) state of the βarr2 shows that the C-domain undergoes : (A) a ~18° twist relative to the N-domain in the presence of DAMGO; (D) a ~20° twist relative to the N-domain in the presence of morphine; (G) a~19° twist relative to the N-domain in the presence of TRV130.

Variation of the interdomain twist with time when the active conformation of the βarr2 fully engages the pp-μOR bound to (B) DAMGO; (E) morphine; (H) TRV130. (C) Distribution of the interdomain twist angle once the active conformation of the βarr2 binds the pp-μOR in the presence of (C) DAMGO; (F) morphine; (I) TRV130.

(J) RMSD variation of the βarr2-pp-μOR complex with time. Here, the RMSD for the backbone atoms of the whole structures over the course of simulation are compared to the initial trajectory.

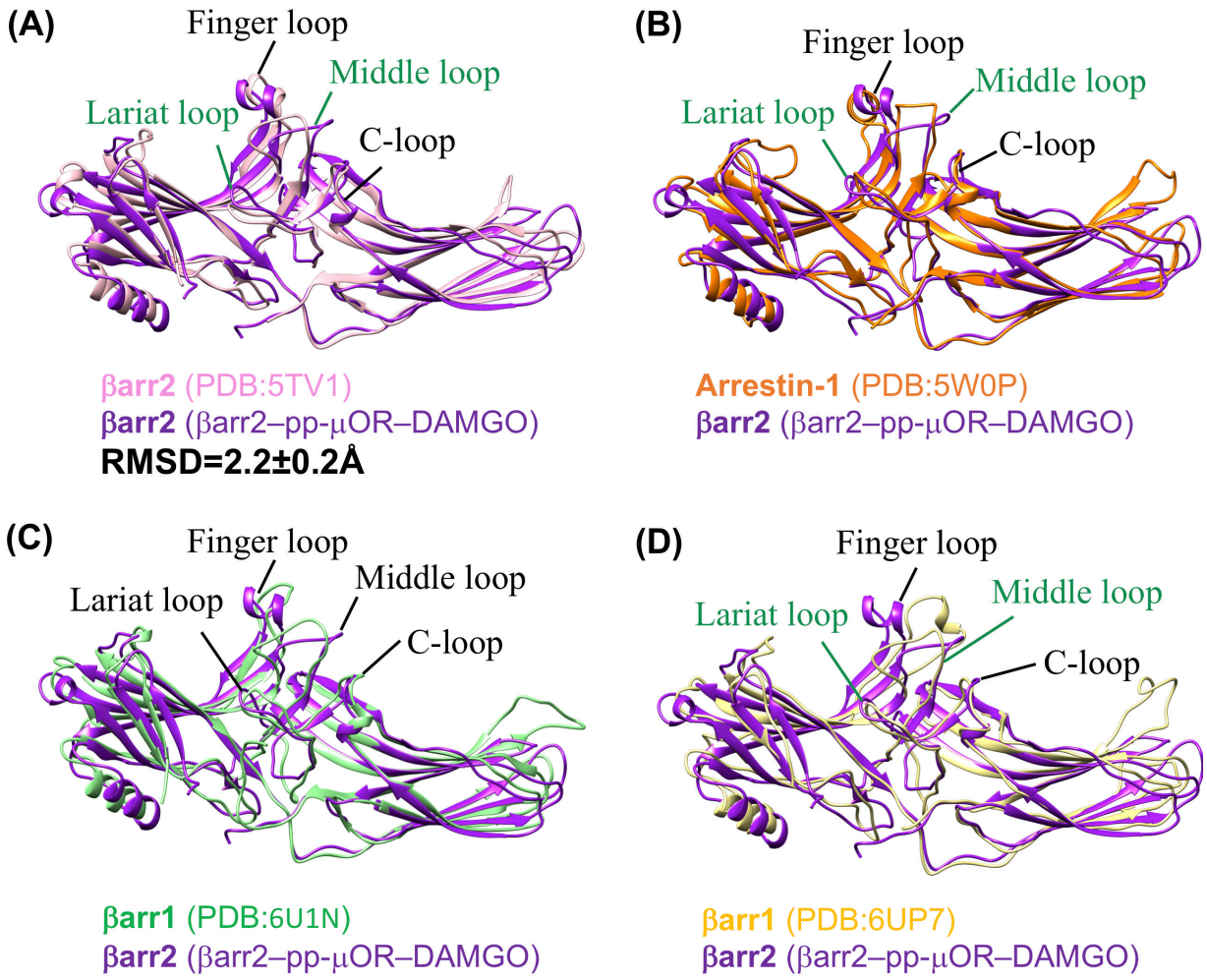

Fig. S3. The comparison of the active conformation of the βarr2 in complex with the pp-μOR bound to DAMGO (obtained from our MD simulation) with the experimentally resolved active conformation of: (A) βarr2 (PDB:5TV1); (B) Arrestin-1 in the complex of pp-rhod1-arrestin-1 (PDB:5W0P); (C) βarr1 in the complex of pp-M2 muscarinic receptor-βarr1 (PDB:6U1N); and (D) βarr1 in the complex of pp-neurotensin receptor 1-βarr1 (PDB:6UP7).

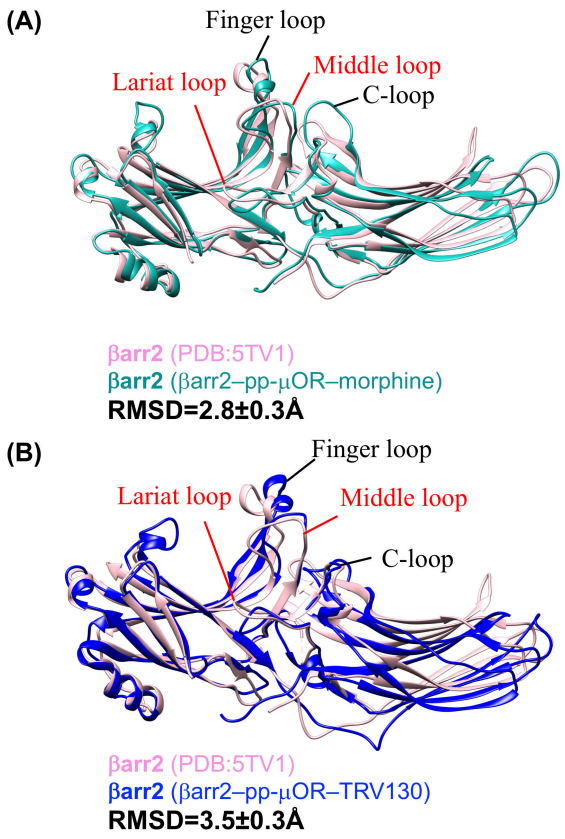

Fig. S4. The comparison between the experimentally resolved active conformation of βarr2 with the active conformation of the βarr2 (obtained from our MD simulations) in complex with the pp-μOR bound to (A) morphine, and (B) TRV130.

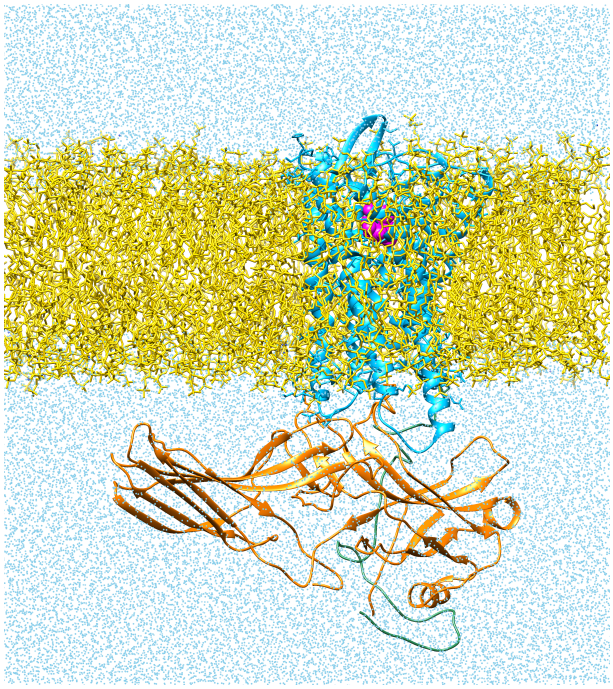

Fig. S5. Phosphorylated human μOR-βarr2-morphine complex immersed in the lipid bilayer depicted. Here, we eliminated the lipid anchoring from the C-edge. Cartoon views colored by subunit: blue, pp-μOR; Orange, -βarr2; magenta, MP1104; green, pp-C tail; sky blue dots, water; yellow, POPC. This system contains 356 POPC molecules, ~40K water molecules, and excess 0.15mM of NaCl counterions.

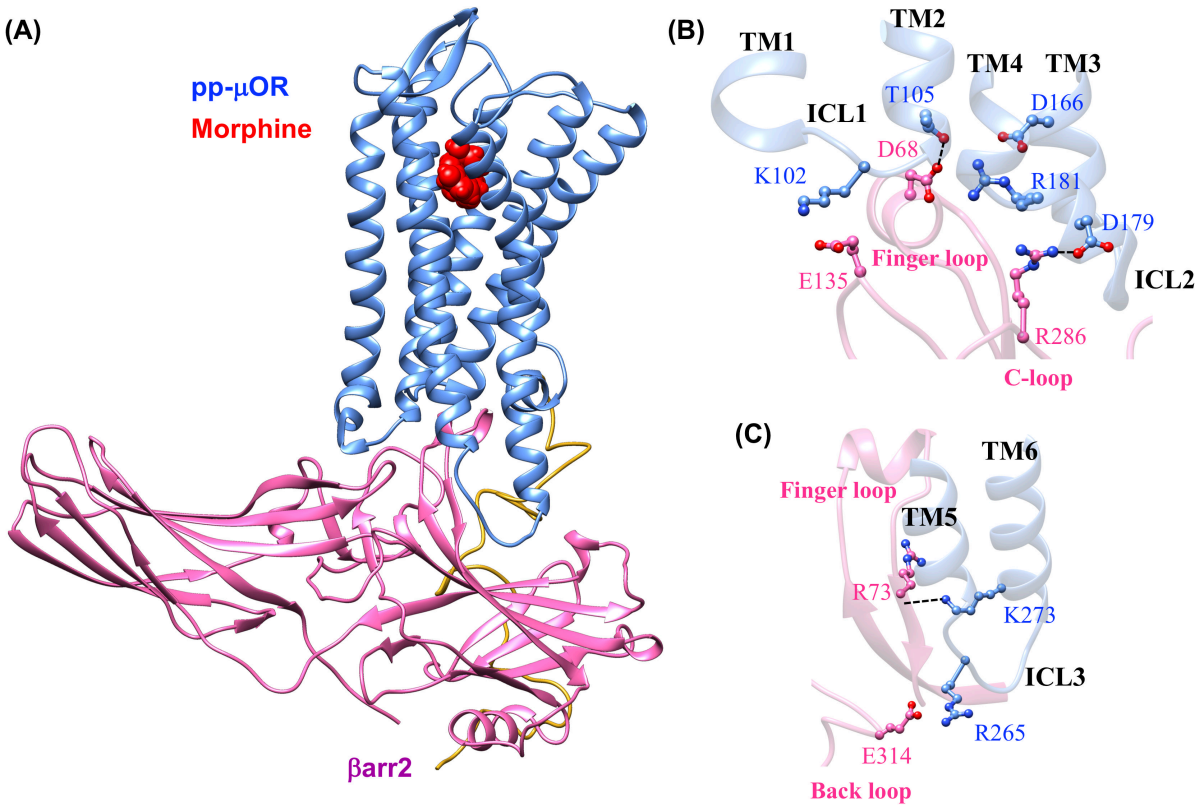

Fig. S6. (A) The high affinity βarr2-pp-μOR-morphine complex immersed in the membrane bilayer obtained independently form the second 500 ns of MD simulation. (B) The polar anchor from the βarr2 to ICL2 of the μOR, which creates a polar network of interactions from the finger loop to ICL2 and the cytosolic end of TM2. (E) polar anchors from the βarr2 to both ICL3 and the bottom end of TM6, fully engaging the body of the βarr2 to the core of the μOR.

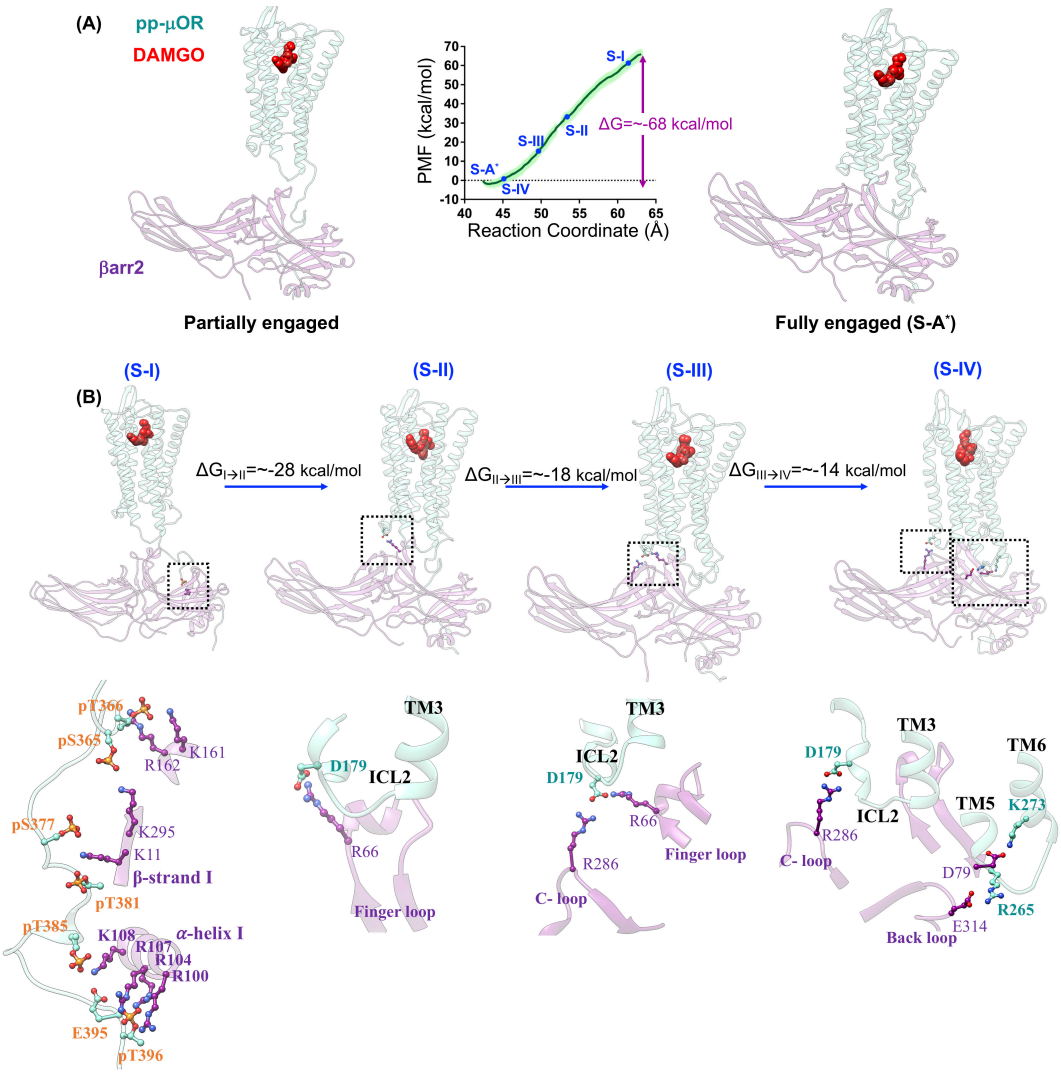

Fig. S7. Process of forming the fully engaged complex between the pp-μOR and the βarr2 in the presence of DAMGO. (A) The averaged PMF indicates that the recruited βarr2 by the pp-C tail spontaneously couples the core of pp-μOR. The free energy was obtained by umbrella sampling, where the reaction coordinate is the distance along the z-component between the center of mass of Cαs in the pp-μOR for residues 54-340 and the center of mass of Cαs in βarr2. The errors were shown as shaded profile in light green. (B) Sequence of important events in the recruitment of the βarr2 by the pp-μOR bound to DAMGO. Our free energy calculation suggests the following pathway; i) S-I: the βarr2 couples to the pp-C tail of μOR, involving mainly salt bridges from pS and pT residues to positively charged residues on the N-domain of the βarr2; ii) S-II: the flexible finger loop extends to the receptor core to engage the ICL2 by forming a salt bridge from R66 to D179; iii) S-III: the extended finger loop induces D179 to form an ionic anchor with $R286^{\text{Back loop}}$. iv) S-IV: anchoring to the ICL2 allows the rest of βarr2 to ascend to form two anchors from E314 to R265 on the ICL3 and from D79 to $K273^{6.26}$. This free energy calculation indicates that the finger loop is a main driver of the βarr2 coupling to the 7TM core of pp-μOR.

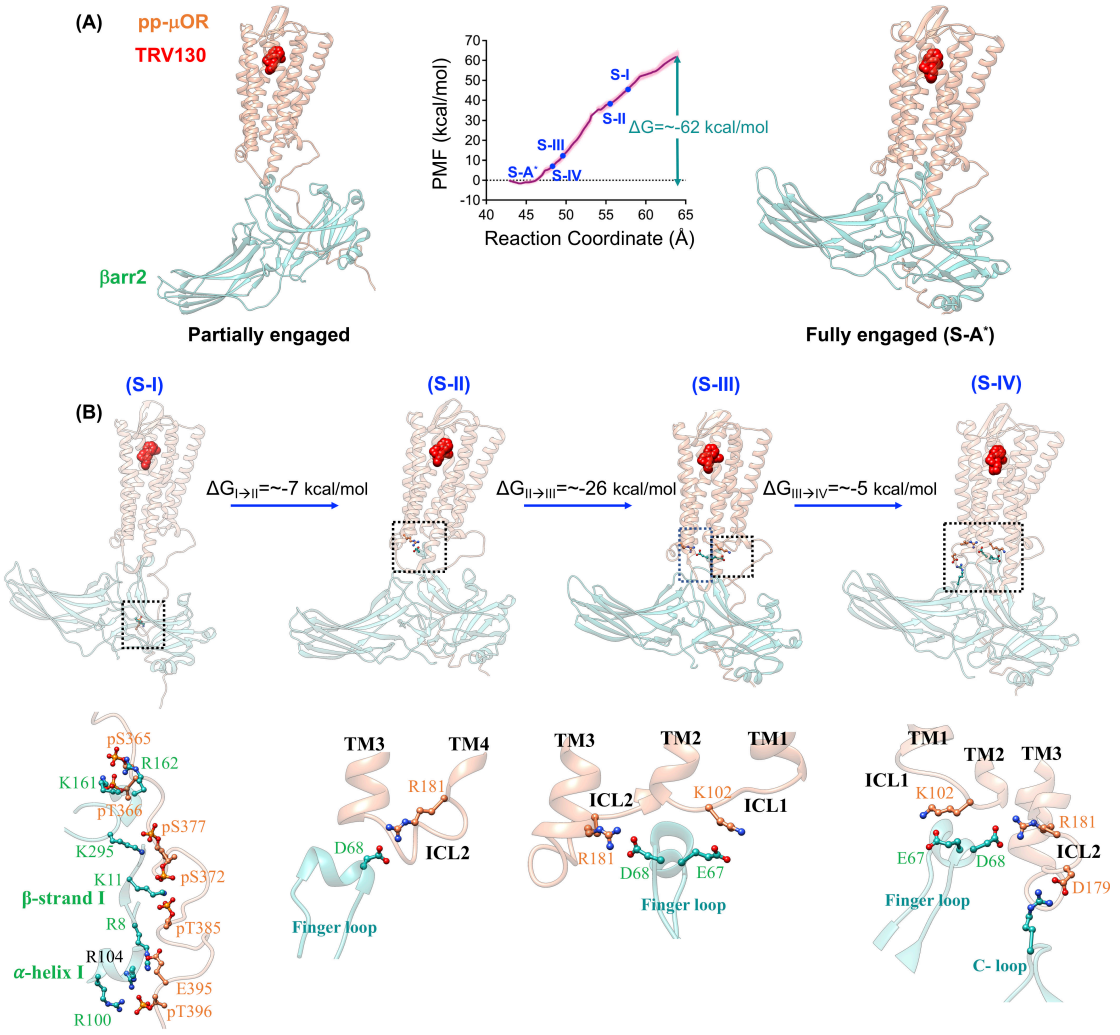

Fig. S8. Process of forming the fully engaged complex between the pp-μOR and the βarr2 in the presence of TRV130. (A) The averaged PMF indicates that the recruited βarr2 by the pp-C tail spontaneously couples the core of pp-μOR. The free energy was obtained by umbrella sampling, where the reaction coordinate is the distance along the z-component between the center of mass of Cαs in the pp-μOR for residues 54-340 and the center of mass of Cαs in βarr2. The errors were shown as shaded profile in pink. (B) Sequence of important events in the recruitment of the βarr2 by the pp-μOR bound to TRV130. Our free energy calculation suggests the following pathway; i) S-I: the βarr2 couples to the pp-C tail of μOR, involving mainly salt bridges from pS and pT residues to positively charged residues on the N-domain of the βarr2; ii) S-II: the flexible finger loop extends to the receptor core to engage the ICL2 by forming a salt bridge from D68 to R181; iii) S-III: the extended finger loop moves toward the ICL1 to form an additional salt bridge from E67 to K102ICL2. Anchoring to the ICL1 allows the rest of βarr2 to ascend to form an ionic anchor from R286 on the C-loop to D179 on the ICL2. Our free energy calculation for the third case study confirms that the finger loop is a main driver of the βarr2 coupling to the 7TM core of pp-μOR.

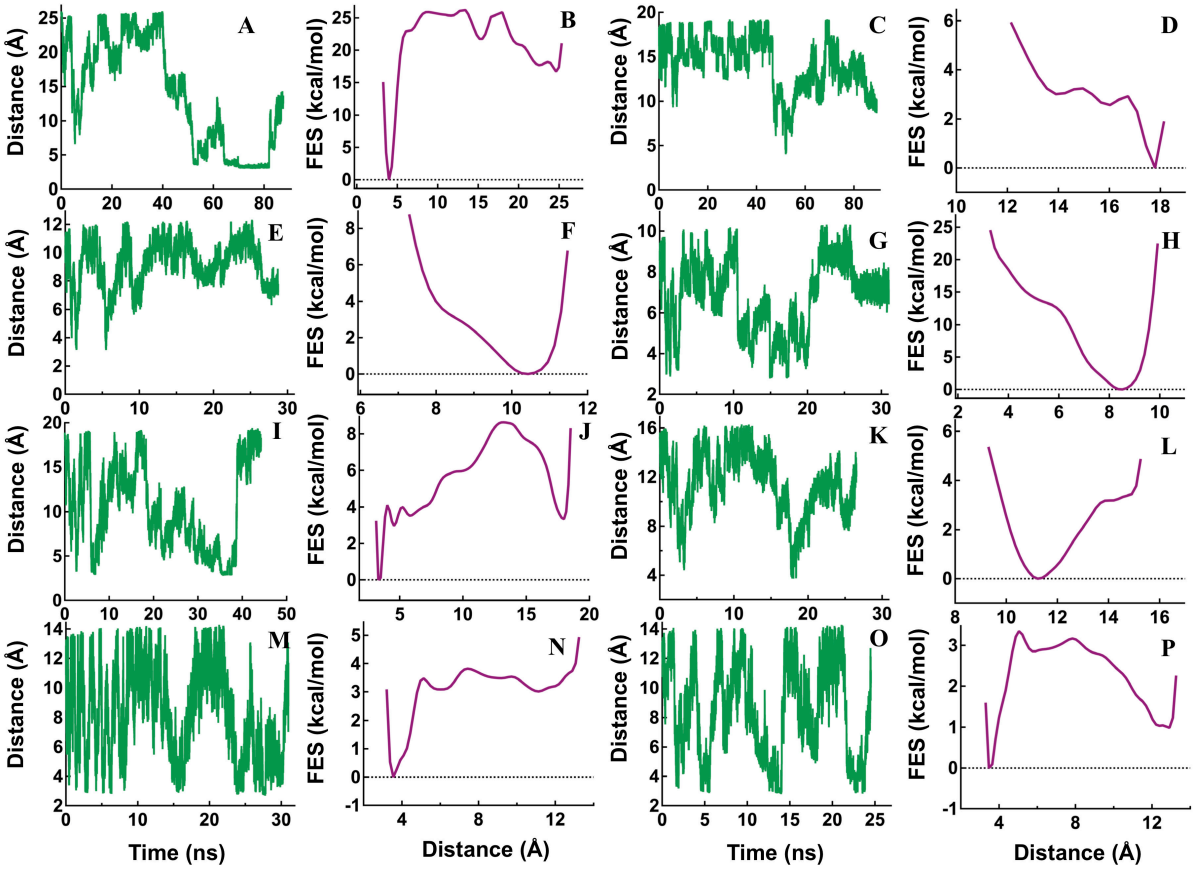

Fig. S9. Optimization of pp-C tail conformation in complex with inactive state of βarr2 using metaMD simulations. Calculated affinity free energy profile by metaMD for interactions: (B) pT396(P)-R95βarr2(CZ); (D) pT372 (P)-R47βarr2(CZ); (F) pS365(P)-K13βarr2(NZ); (H) pS377(P)-K13βarr2(NZ); (J) pT385(P)-K6βarr2(NZ); (L) pT372 (P)-R47βarr2(CZ); (N) pT372 (P)-K148βarr2(NZ); (P) pS358(P)-K153βarr2(NZ). Variations of interactions with time between (A) pT396(P)-R95βarr2(CZ); (C) pT372 (P)-R47βarr2(CZ); (E) pS365(P)-K13βarr2(NZ); (G) pS377(P)-K13βarr2(NZ); (I) pT385(P)-K6βarr2(NZ); (K) pT372 (P)-R47βarr2(CZ); (M) pT372 (P)-K148βarr2(NZ); (O) pS358(P)-K153βarr2(NZ).

Table S1. List of metaMD simulation along with the conditions used to evaluate free energies to optimize the conformation of pp-C tail in the presence of inactive state of βarr2.

Calculation #	Duration (ns)	Reaction coordinate (Å)	Initial value (Å)	Starting point (ns)	MetaMD parameters	Restraint
1	87.5	pT396(P)-R95$^{\beta arr2}$(CZ)	25.6	-	Hills height=0.6 kcal.mol^{-1},σ=1Å, Bias factor=20	D179(CG)-K134 $^{\beta arr2}$ (NZ)
2	89.3	pT372 (P)-R47$^{\beta arr2}$(CZ)	18.1	~69.7 (from #1)	Hills height=0.6 kcal.mol^{-1},σ=1Å, Bias factor=20	1) D179(CG)-K134 $^{\beta arr2}$ (NZ) 2) pT396(P)-R95$^{\beta arr2}$ (CZ)
3	28.7	pS365(P)-K13$^{\beta arr2}$(NZ)	10.3	~26.1 (from #2)	Hills height=0.6 kcal.mol^{-1},σ=1Å, Bias factor=20	1) D179(CG)-K134 $^{\beta arr2}$ (NZ) 2) pT396(P)-R95$^{\beta arr2}$ (CZ)
4	46.0	pS377(P)-K13$^{\beta arr2}$(NZ)	8.6	~26.1 (from #3)	Hills height=0.6 kcal.mol^{-1},σ=0.5Å, Bias factor=20	1) D179(CG)-K134 $^{\beta arr2}$ (NZ) 2) pT396(P)-R95$^{\beta arr2}$ (CZ)
5	44.2	pT385(P)-K6$^{\beta arr2}$(NZ)	18.7	~32.8 (from #4)	Hills height=0.6 kcal.mol^{-1},σ=0.5Å, Bias factor=20	1) D179(CG)-K134 $^{\beta arr2}$ (NZ) 2) pT396(P)-R95$^{\beta arr2}$ (CZ)
6	26.5	pT372 (P)-R47$^{\beta arr2}$(CZ)	15.3	~35.2 (from #5)	Hills height=0.6 kcal.mol^{-1},σ=0.5Å, Bias factor=20	1) D179(CG)-K134 $^{\beta arr2}$ (NZ) 2) pT396(P)-R95$^{\beta arr2}$ (CZ) 3) pT385(P)-K6$^{\beta arr2}$(NZ)
7	31.0	pT372 (P)-K148$^{\beta arr2}$(NZ)	12.9	~26.4 (from #6)	Hills height=0.6 kcal.mol^{-1},σ=0.5Å, Bias factor=20	1) D179(CG)-K134 $^{\beta arr2}$ (NZ) 2) pT396(P)-R95$^{\beta arr2}$ (CZ) 3) pT385(P)-K6$^{\beta arr2}$(NZ)
8	24.5	pS358(P)-K153$^{\beta arr2}$(NZ)	13.0	~30.2(from #7)	Hills height=0.6 kcal.mol^{-1},σ=0.5Å, Bias factor=20	1) D179(CG)-K134 $^{\beta arr2}$ (NZ) 2) pT396(P)-R95$^{\beta arr2}$ (CZ) 3) pT385(P)-K6$^{\beta arr2}$(NZ) 4) pT372 (P)-K148$^{\beta arr2}$(NZ) 5) pT372 (P)-R47$^{\beta arr2}$(CZ) 6) pS377(P)-K13$^{\beta arr2}$(NZ)

Movie S1 (separate file). βarr2 recruitment by pp-μOR and morphine.

Movie S2 (separate file). Finger loop as a major driver of βarr2 coupling to the core pp-μOR.

Movie S3 (separate file). Emergence of polar anchor between βarr2 and ICL3 of pp-μOR.

Movie S4 (separate file). Emergence of polar anchor between βarr2 and ICL2 of pp-μOR.

SI References

1. X. E. Zhou, Y. He, P. W. de Waal, X. Gao, Y. Kang, N. Van Eps, Y. Yin, K. Pal, D. Goswami, T. A. White, Identification of phosphorylation codes for arrestin recruitment by G protein-coupled receptors. *Cell*. **170**, 457–469 (2017).

2. N. Guex, M. C. Peitsch, SWISS-MODEL and the Swiss-Pdb Viewer: an environment for comparative protein modeling. *electrophoresis*. **18**, 2714–2723 (1997).

3. B. Webb, A. Sali, in *Functional Genomics* (Springer, 2017), pp. 39–54.

4. Y. Kang, X. E. Zhou, X. Gao, Y. He, W. Liu, A. Ishchenko, A. Barty, T. A. White, O. Yefanov, G. W. Han, Crystal structure of rhodopsin bound to arrestin by femtosecond X-ray laser. *Nature*. **523**, 561 (2015).

5. W. Huang, A. Manglik, A. J. Venkatakrishnan, T. Laeremans, E. N. Feinberg, A. L. Sanborn, H. E. Kato, K. E. Livingston, T. S. Thorsen, R. C. Kling, Structural insights into μ-opioid receptor activation. *Nature*. **524**, 315–321 (2015).

6. J. K. Bray, R. Abrol, W. A. Goddard, B. Trzaskowski, C. E. Scott, SuperBiHelix method for predicting the pleiotropic ensemble of G-protein–coupled receptor conformations. *Proc. Natl. Acad. Sci.* **111**, E72–E78 (2014).

7. V. W. Tak Kam, W. A. Goddard III, Flat-bottom strategy for improved accuracy in protein side-chain placements. *J. Chem. Theory Comput.* **4**, 2160–2169 (2008).

8. A. R. Griffith, thesis, California Institute of Technology (2017).

9. X. Zhan, L. E. Gimenez, V. V. Gurevich, B. W. Spiller, Crystal structure of arrestin-3 reveals the basis of the difference in receptor binding between two non-visual subtypes. *J. Mol. Biol.* **406**, 467–478 (2011).

10. A. Waterhouse, M. Bertoni, S. Bienert, G. Studer, G. Tauriello, R. Gumienny, F. T. Heer, T. A. P. de Beer, C. Rempfer, L. Bordoli, SWISS-MODEL: homology modelling of protein structures and complexes. *Nucleic Acids Res.* **46**, W296–W303 (2018).

11. R. Casasnovas, V. Limongelli, P. Tiwary, P. Carloni, M. Parrinello, Unbinding kinetics of a p38 MAP kinase type II inhibitor from metadynamics simulations. *J. Am. Chem. Soc.* **139**, 4780–4788 (2017).

12. P. Tiwary, V. Limongelli, M. Salvalaglio, M. Parrinello, Kinetics of protein–ligand unbinding: Predicting pathways, rates, and rate-limiting steps. *Proc. Natl. Acad. Sci.* **112**, E386–E391 (2015).

13. A. Barducci, G. Bussi, M. Parrinello, Well-tempered metadynamics: a smoothly converging and tunable free-energy method. *Phys. Rev. Lett.* **100**, 020603 (2008).

14. G. A. Tribello, M. Bonomi, D. Branduardi, C. Camilloni, G. Bussi, PLUMED 2: New feathers for an old bird. *Comput. Phys. Commun.* **185**, 604–613 (2014).

15. A. Koehl, H. Hu, S. Maeda, Y. Zhang, Q. Qu, J. M. Paggi, N. R. Latorraca, D. Hilger, R. Dawson, H. Matile, Structure of the μ-opioid receptor–Gi protein complex. *Nature*. **558**, 547–552 (2018).

16. S. B. Needleman, C. D. Wunsch, A general method applicable to the search for similarities in the amino acid sequence of two proteins. *J. Mol. Biol.* **48**, 443–453 (1970).

17. G. N. Patey, J. P. Valleau, The free energy of spheres with dipoles: Monte Carlo with multistage sampling. *Chem. Phys. Lett.* **21**, 297–300 (1973).

18. G. M. Torrie, J. P. Valleau, Nonphysical sampling distributions in Monte Carlo free-energy estimation: Umbrella sampling. *J. Comput. Phys.* **23**, 187–199 (1977).

19. S. Kumar, J. M. Rosenberg, D. Bouzida, R. H. Swendsen, P. A. Kollman, The weighted histogram analysis method for free-energy calculations on biomolecules. I. The method. *J. Comput. Chem.* **13**, 1011–1021 (1992).

20. J. S. Hub, B. L. De Groot, D. Van Der Spoel, g_wham□ A Free Weighted Histogram Analysis Implementation Including Robust Error and Autocorrelation Estimates. *J. Chem. Theory Comput.* **6**, 3713–3720 (2010).

21. E. F. Pettersen, T. D. Goddard, C. C. Huang, G. S. Couch, D. M. Greenblatt, E. C. Meng, T. E. Ferrin, UCSF Chimera—a visualization system for exploratory research and analysis. *J. Comput. Chem.* **25**, 1605–1612 (2004).

22. A. Mafi, S.-K. Kim, W. A. Goddard, The atomistic level structure for the activated human κ-opioid receptor bound to the full Gi protein and the MP1104 agonist. *Proc. Natl. Acad. Sci.* **117**, 5836–5843 (2020).